Cell Metabolism
Short Article

Desnutrin/ATGL Is Regulated by AMPK and Is Required for a Brown Adipose Phenotype

Maryam Ahmadian,[1] Marcia J. Abbott,[1] Tianyi Tang,[1] Carolyn S.S. Hudak,[1] Yangha Kim,[1] Matthew Bruss,[1] Marc K. Hellerstein,[1] Hui-Young Lee,[3] Varman T. Samuel,[3] Gerald I. Shulman,[3,4,5] Yuhui Wang,[1] Robin E. Duncan,[1] Chulho Kang,[2] and Hei Sook Sul[1,*]
[1]Department of Nutritional Science and Toxicology
[2]Department of Molecular and Cell Biology
University of California, Berkeley, Berkeley, CA 94720, USA
[3]Department of Internal Medicine
[4]Department of Cellular and Molecular Physiology
[5]Howard Hughes Medical Institute
Yale University School of Medicine, New Haven, CT 06510, USA
*Correspondence: hsul@berkeley.edu
DOI 10.1016/j.cmet.2011.05.002

SUMMARY

While fatty acids (FAs) released by white adipose tissue (WAT) provide energy for other organs, lipolysis is also critical in brown adipose tissue (BAT), generating FAs for oxidation and UCP-1 activation for thermogenesis. Here we show that adipose-specific ablation of desnutrin/ATGL in mice converts BAT to a WAT-like tissue. These mice exhibit severely impaired thermogenesis with increased expression of WAT-enriched genes but decreased BAT genes, including UCP-1 with lower PPARα binding to its promoter, revealing the requirement of desnutrin-catalyzed lipolysis for maintaining a BAT phenotype. We also show that desnutrin is phosphorylated by AMPK at S406, increasing TAG hydrolase activity, and provide evidence for increased lipolysis by AMPK phosphorylation of desnutrin in adipocytes and in vivo. Despite adiposity and impaired BAT function, desnutrin-ASKO mice have improved hepatic insulin sensitivity with lower DAG levels. Overall, desnutrin is phosphorylated/activated by AMPK to increase lipolysis and brings FA oxidation and UCP-1 induction for thermogenesis.

INTRODUCTION

Adipose tissue plays a critical role in controlling energy balance. As the primary fuel reserve in mammals, white adipose tissue (WAT) has the unique function of storing triacylglycerol (TAG) for hydrolysis (lipolysis) to provide fatty acids (FAs) for other organs during times of energy shortage (Ahmadian et al., 2009a). Brown adipose tissue (BAT), on the other hand, is specialized in thermogenesis, using FAs generated by lipolysis for activation of UCP-1 and for mitochondrial β-oxidation (Cannon and Nedergaard, 2004). These two adipose tissues can be distinguished from each other based on their morphology, gene expression profile, and characteristic biochemical functions (Frontini and Cinti, 2010). Under certain conditions, such as chronic cold exposure, not only is the thermogenic capacity of BAT increased, but WAT can also be converted to a BAT-like tissue (Frontini and Cinti, 2010). In contrast, while BAT is abundant in newborns, the majority is transformed to WAT in adult humans. Yet how these conversions between BAT and WAT occur is not well understood (Frontini and Cinti, 2010).

It is clear that lipolysis is a critical metabolic process in both WAT and BAT. Lipolysis occurs in three stages, with different enzymes acting at each step: TAG is hydrolyzed to form diacylglycerol (DAG), catalyzed by desnutrin/ATGL/iPLA$_2\zeta$ (gene name: PNPLA2, TTS2.2), which we and others identified as the major TAG hydrolase in adipose tissue, but which is also expressed in other tissues (Villena et al., 2004a; Jenkins et al., 2004; Zimmermann et al., 2004). DAG is then hydrolyzed by hormone-sensitive lipase (HSL) to monoacylglycerol and, subsequently, glycerol, with a FA released at each stage (Duncan et al., 2007). Regulation of lipolysis by catecholamine stimulation of Gα_s-coupled β-adrenergic receptors, resulting in PKA phosphorylation of HSL and perilipin, is well characterized (Ahmadian et al., 2009a). Yet how desnutrin is regulated by phosphorylation is not known. Mass spectrometry analysis identified two serine residues in murine desnutrin that are phosphorylated (Kim et al., 2006). However, PKA does not appear to phosphorylate desnutrin (Zimmermann et al., 2004). Another kinase that plays a critical role in maintaining energy balance is AMP-activated protein kinase (AMPK), a serine/threonine kinase that is activated during a low-energy state (Lage et al., 2008). However, its role in regulating lipolysis in adipose tissue has been controversial, and whether it phosphorylates mammalian desnutrin is unknown (Daval et al., 2005; Yin et al., 2003).

We previously found that adipose overexpression of desnutrin in mice increases lipolysis, FA oxidation within adipose tissue, and thermogenesis, resulting in higher energy expenditure and resistance to obesity (Ahmadian et al., 2009b). Global ablation of desnutrin/ATGL in mice results in massive TAG accumulation in multiple organs, causing premature death (Haemmerle et al., 2006). Thus, adipose-specific ablation of desnutrin is required to determine its adipose-autonomous effects on BAT and WAT and its role in obesity. Here we report that adipose-specific ablation of desnutrin (desnutrin-ASKO) not only manifests in obesity

but converts BAT to a WAT-like tissue. Thus, desnutrin-ASKO mice exhibit impaired thermogenesis with decreased expression of UCP-1, with lower PPARα binding to its promoter, revealing the requirement of desnutrin-catalyzed lipolysis in the maintenance of a BAT phenotype. We also show that desnutrin is phosphorylated at S406 by AMPK, to increase its TAG hydrolase activity, and provide evidence for regulation of lipolysis by AMPK phosphorylation of desnutrin in both cultured adipocytes and in vivo in mice. We conclude that desnutrin is phosphorylated by AMPK to increase lipolysis and that desnutrin-catalyzed lipolysis brings FA oxidation and UCP-1 induction for thermogenesis.

RESULTS

Diet-Induced Obesity in Desnutrin-ASKO Mice Results from Blunted Lipolysis and Impaired Thermogenesis

We generated adipose-specific desnutrin knockout mice (desnutrin-ASKO mice) using the Flp-Cre strategy, and these mice were compared to control, flox/flox littermates for all experiments (Figures 1A and S1A–S1C). Desnutrin protein in WAT and BAT was easily detected in control, flox/flox mice but was barely detectable in desnutrin-ASKO mice (Figure 1B, upper). In other organs, such as the heart and liver, desnutrin protein levels were unchanged compared to control mice (Figure 1B, middle). RT-qPCR also detected minimal changes in desnutrin expression in macrophages, compared to the drastic decrease in BAT (Figure 1B, lower).

By 5 weeks of age, desnutrin-ASKO mice on a HFD showed a trend toward a higher rate of weight gain than flox/flox littermates, reaching statistical significance between 12 and 14 weeks of age (Figures 1C and S1D, right). Increased weight gain and fat pad weights were also observed in desnutrin-ASKO mice on chow diet, albeit to a lesser extent (Figures S1D, left, and S1E). However, desnutrin-ASKO mice consumed the same amount of food as flox/flox littermates (Figure 1E, inset). Liver, kidney, and heart weights were similar and therefore could not account for the higher body weights in desnutrin-ASKO mice (Figure 1F). On the other hand, after 20 weeks on a HFD, gonadal, inguinal, and renal WAT depot weights were 1.4-, 2.0-, and 1.9-fold higher, respectively, in desnutrin-ASKO mice compared to control mice (Figure 1E). BAT was even more affected than WAT, with weights 4.9-fold higher, and resembling WAT in terms of its pale color (Figures 1D and 1E). Histological analysis revealed a greater frequency of larger adipocytes in gonadal fat pads from desnutrin-ASKO mice, indicating increased adipocyte size (Figure 1G, left). Brown adipocyte size was also markedly increased in desnutrin-ASKO mice (Figure 1G, right).

Expression levels of early as well as late markers of adipocyte differentiation in WAT of desnutrin-ASKO mice were not changed, indicating normal adipocyte differentiation (Figure S1F). Glycerol release was drastically decreased in WAT of desnutrin-ASKO mice compared to control mice under both basal and isoproterenol-stimulated conditions (Figure 2A, left). Although not significantly different under basal conditions in WAT, FA release was decreased by 22% after 2 hr and 41% after 4 hr in WAT of desnutrin-ASKO mice under isoproterenol-stimulated conditions (Figure 2A, right). In isolated adipocytes, we detected decrease in FA release under both basal and stimulated conditions (Figure 2B). Lipolysis was also severely blunted in BAT of desnutrin-ASKO mice, being decreased by 60% under basal conditions (Figure 2C). Next, using a heavy water labeling technique, we measured in vivo TAG turnover and de novo palmitate turnover in WAT and BAT. While TAG turnover was 24% after 6 days in WAT of control mice, it was only 7% in desnutrin-ASKO mice (Figure 2D, left). Surprisingly, in BAT of control mice, TAG turnover was markedly higher than that in WAT, with a 77% turnover rate after 6 days (Figure 2D, left). However, in BAT of desnutrin-ASKO mice, it was only 29%, which is similar to levels observed in WAT of control mice (Figure 2D, left). Consistent with these findings, de novo palmitate turnover was 8% and 52% in WAT and BAT of control mice, respectively, compared to 3% and 9% in desnutrin-ASKO mice (Figure 2D, right).

We next subjected desnutrin-ASKO mice and flox/flox littermates to cold exposure in the fasted state. While control mice were able to maintain body temperature well into 5 hr at 4°C, desnutrin-ASKO mice quickly reached life-threatening hypothermia after just 90 min (Figure 2E). Cold exposure increased TAG hydrolase activity in BAT of control mice by 2.3-fold, but only 1.4-fold in desnutrin-ASKO mice, indicating the requirement of desnutrin for cold-induced increase in TAG hydrolase activity (Figure 2F). Notably, we did not observe any changes in desnutrin protein levels in BAT after cold exposure, suggesting that desnutrin activity may be regulated in BAT by posttranslational modification (Figure 2F, inset). There was no change in ambulatory activity (data not shown). However, total oxygen consumption was decreased in desnutrin-ASKO mice compared to flox/flox littermates (Figure 2G). In response to the β_3-agonist, CL316243, flox/flox mice exhibited a drastic increase in their metabolic rate, as indicated by oxygen consumption, whereas desnutrin-ASKO mice showed no change, revealing a blunted β_3-adrenergic response (Figure 2H). Accordingly, we found that FA oxidation was blunted in both white and brown adipocytes from desnutrin-ASKO mice (Figure 2I). Despite adiposity and impaired BAT function, desnutrin-ASKO mice have improved hepatic insulin sensitivity with lower DAG levels (Figures S2A–S2I).

Desnutrin Ablation Promotes the Conversion of BAT to a WAT-like Tissue

Transmission electron microscopy showed that while BAT from flox/flox mice had numerous small lipid droplets, BAT from desnutrin-ASKO mice contained larger, but fewer lipid droplets (Figure 3A). We also observed fewer mitochondria in BAT from desnutrin-ASKO mice, and the majority of mitochondria were composed of randomly oriented cristae, characteristic of WAT, compared to the classic laminar cristae in BAT from flox/flox mice (Figure 3B). However, morphology of BAT was not altered in desnutrin-ASKO mice at either E17 or E21, suggesting that the conversion of BAT to a WAT-like phenotype in desnutrin-ASKO mice is likely due to the metabolic consequence of decreased desnutrin-catalyzed lipolysis in adults rather than a developmental defect (Figure S3). Furthermore, BAT from desnutrin-ASKO mice showed no changes in the expression of genes that may be critical for BAT development, including Pref-1, C/EBPα, C/EBPδ, PPARγ, and PRDM16 (Figure 3C). In contrast, expression of genes involved in thermogenesis and mitochondrial and peroxisomal FA oxidation, such as ATP5B, COXIV, CPT1β, PHYH, CIDEA, and PPARα, were all decreased

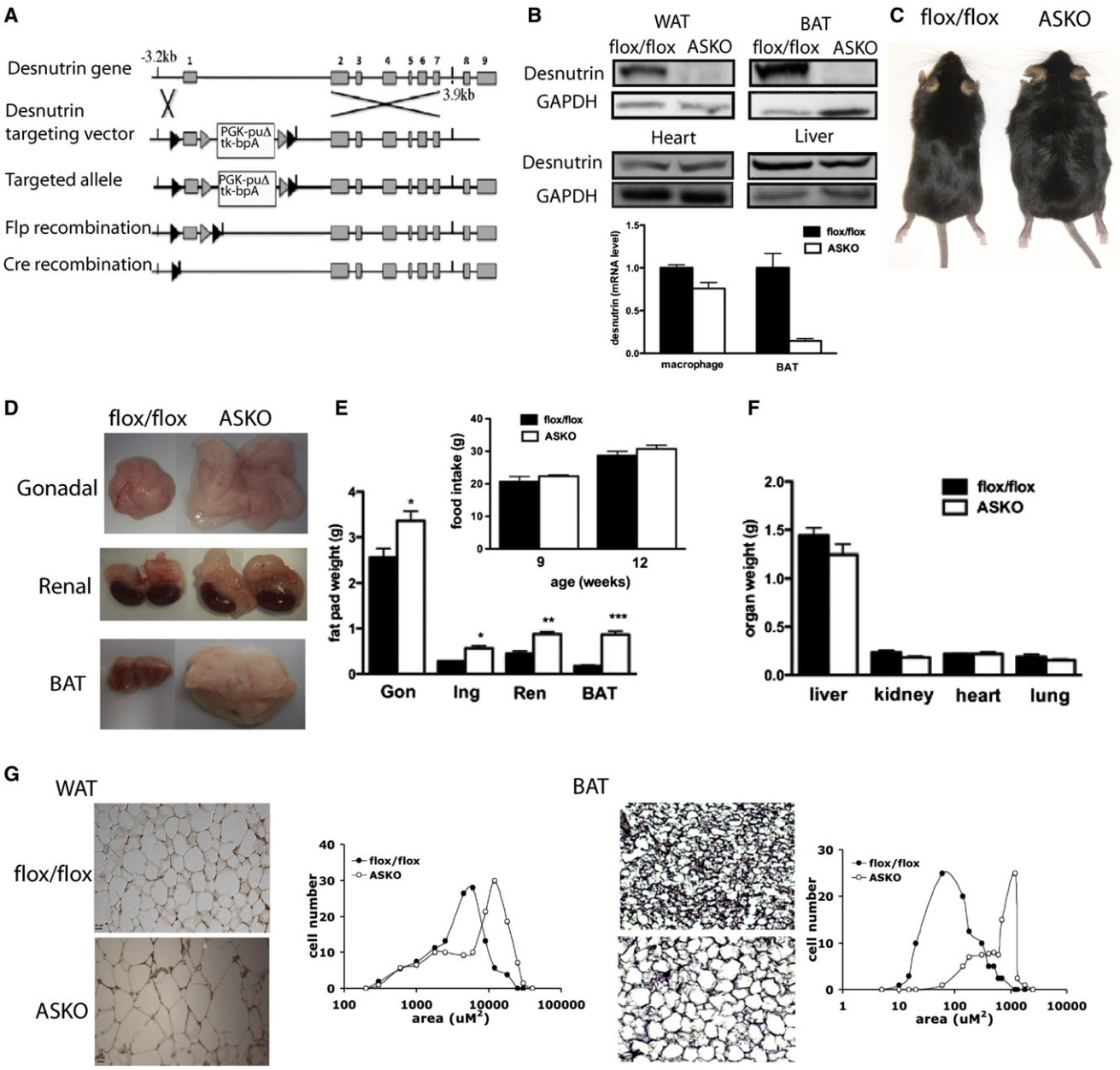

Figure 1. Increased Adiposity in Desnutrin-ASKO Mice

(A) Generation of adipose-specific desnutrin knockout mice.

(B) Western blotting of lysates (40 μg) from WAT, BAT, heart, and liver using a desnutrin antibody (upper) and RT-qPCR for desnutrin expression in the macrophage and BAT (lower).

(C) Male mice on a HFD at 16 weeks of age.

(D) Gonadal, renal, and BAT fat depots (upper, middle, and lower).

(E) Gonadal (Gon), Inguinal (Ing), renal (Ren), and brown adipose tissue (BAT) fat pad weights and food intake (inset) (n = 7).

(F) Liver, kidney, heart, and lung weights (n = 7).

(G) Hematoxylin and eosin-stained paraffin-embedded sections of gonadal WAT (left) and BAT (right) and quantification of cell size. Scale bar (WAT) = 20 μm, scale bar (BAT) = 40 μm. Data are expressed as means ± SEM. *p < 0.05, **p < 0.01, ***p < 0.001.

by 35%–50% (Figure 3D, left). UCP-1 expression was markedly decreased at both the mRNA and protein level (Figures 3D, left, and 3F). RIP140 and CtBP1, transcriptional corepressors that may suppress oxidative and thermogenic genes in adipose tissue, were upregulated in BAT of desnutrin-ASKO mice by 2.8- and 3.5-fold, respectively (Figure 3D, middle) (Frühbeck et al., 2009). In addition, expression of WAT-enriched genes such as Igfbp3, DPT, Hoxc9, and Tcf21 were strongly induced in BAT of desnutrin-ASKO mice (Figure 3D, right). Consistent with our findings in BAT, expression of UCP-1, CPT1β, and

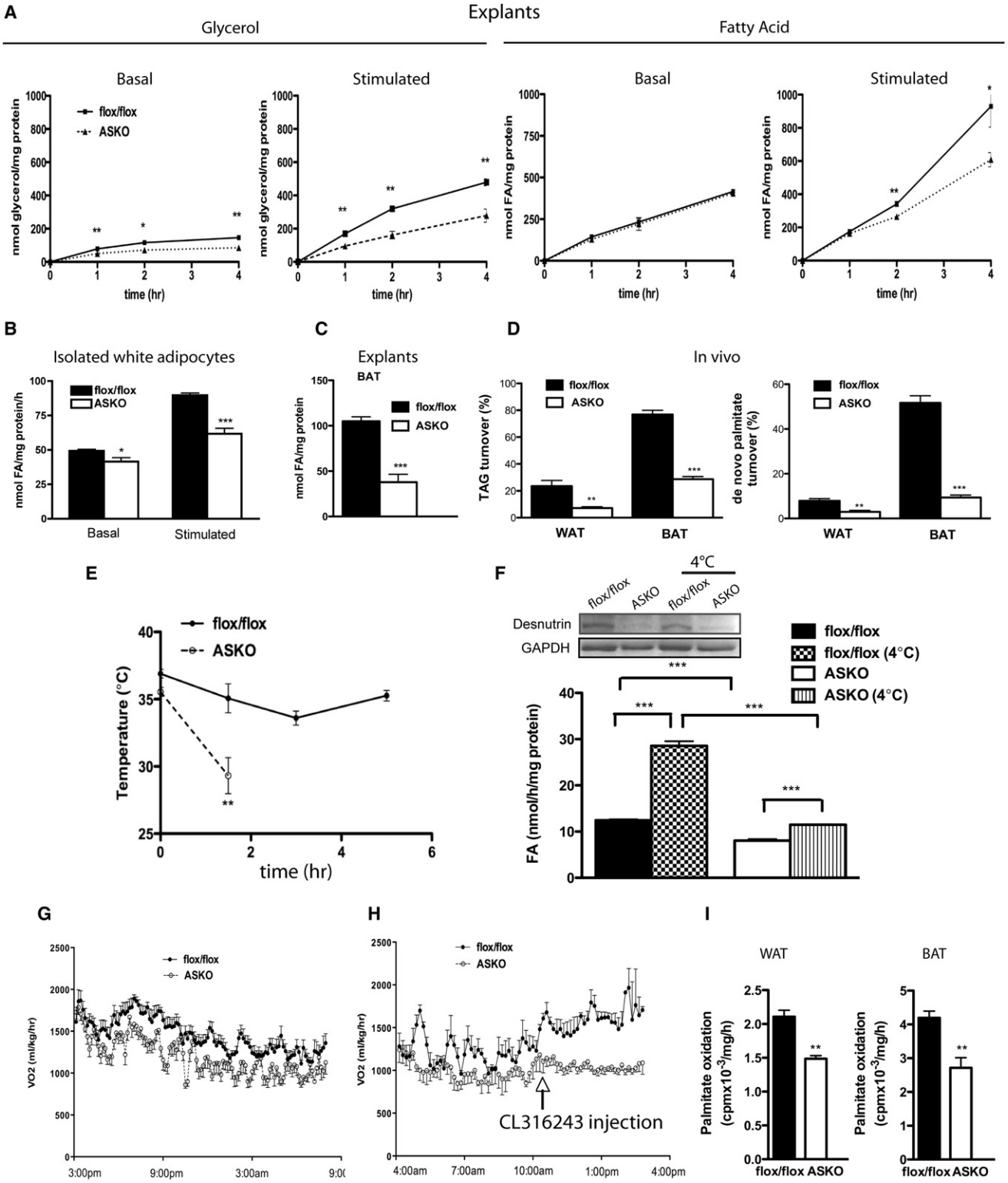

Figure 2. Decreased Lipolysis in Desnutrin-ASKO Mice Results in Impaired Thermogenesis and Energy Expenditure

(A) Glycerol (left) and FA (right) release from explants of gonadal WAT (n = 6).

(B) FA release from isolated white adipocytes.

(C) FA release from explants of BAT (n = 3).

(D) Percent TAG turnover (left) and percent de novo palmitate turnover (right) in gonadal WAT and BAT.

(E) Body temperatures of mice exposed to the cold (4°C) in the fasted state.

PPARα was also decreased in WAT of desnutrin-ASKO mice (Figure 3E).

Lower FA levels within adipocytes due to blunted desnutrin-catalyzed lipolysis in desnutrin-ASKO mice may affect the activity of PPARs to control the expression of many oxidative and thermogenic genes. PPARα, in addition to PPARγ, have been shown to activate the UCP-1 promoter (Barbera et al., 2001). By RT-qPCR, we found that, among the three PPAR members, only PPARα is expressed at a much higher level in BAT compared to WAT (Figure 3G). We detected less PPARα bound to the 2.5 kb enhancer region of the UCP-1 promoter in desnutrin-ASKO mice compared to flox/flox mice (Figure 3H). We also observed lower binding of RIP140 to the UCP-1 promoter in BAT of desnutrin-ASKO mice, despite significantly higher expression levels. Although RIP140 has been reported to play a role in suppressing a BAT phenotype, our results suggest that impaired binding of PPARα may have precluded binding of this corepressor in our desnutrin-ASKO mice. Similar to our findings in BAT of desnutrin-ASKO mice, we found that the expression of UCP-1, CIDEA, COXIV, and CPT1β were all decreased in BAT of PPARα null mice (Figure 3I). Furthermore, PPARα null mice were also unable to maintain body temperature during cold exposure (Figure 3J). Additionally, adipocyte FA oxidation was also blunted in these mice (Figure 3K). Our finding that PPARα null mice phenocopy desnutrin-ASKO in regards to thermogenesis suggests that desnutrin-catalyzed lipolysis may activate PPARα to promote thermogenesis.

AMPK Phosphorylates Desnutrin to Increase Its TAG Hydrolase Activity

Cold exposure and β-agonist treatment induce the thermogenic capacity of BAT, which is mediated primarily through PKA signaling. However, desnutrin does not appear to be phosphorylated by PKA (Zimmermann et al., 2004). In *C. elegans*, desnutrin was reported to be phosphorylated by AMPK to inhibit its lipase activity to conserve energy during dauer (Narbonne and Roy, 2009). However, the AMPK phosphorylation site identified in *C. elegans* is not conserved in mammalian desnutrin. Mass spectrometry analysis detected two phosphorylated serine residues in murine desnutrin (S406 and S430) (Kim et al., 2006). We speculated that, being a perfect AMPK consensus site, S406 might be an AMPK phosphorylation site (Figure 4A). We thus attempted to in vitro phosphorylate desnutrin, which was immunoprecipitated from HEK293 cells transfected with desnutrin expression vector, using purified AMPK and [γ-^{32}P]ATP. Indeed, we detected phosphorylation of desnutrin by AMPK in vitro (Figure 4B). To identify the specific site(s) of desnutrin that AMPK phosphorylates, we generated nonphosphorylatable alanine mutant forms of desnutrin at the two putative phosphorylation sites (S406A and S430A) and used them for in vitro phosphorylation. While WT and the S430A desnutrin mutant were phosphorylated by AMPK, the S406A mutant was not, indicating S406 of desnutrin to be a unique and bona fide AMPK phosphorylation site (Figures 4B and 4C). Interestingly, we also found the amino acid sequence at S406 of desnutrin to be a perfect 14-3-3 binding motif. A specific 14-3-3 phospho-binding peptide antibody detected WT desnutrin but not the S406 mutant (Figure 4B). Furthermore, we could detect a direct interaction between desnutrin and 14-3-3 by pull-down assay using GST-14-3-3 and in vitro translated product of desnutrin (Figure 4D), but not when desnutrin product was first treated with alkaline phosphatase, demonstrating its dependence on desnutrin phosphorylation.

Next, we transfected HEK293 cells with desnutrin and treated them with the cell-permeable AMPK-activator, AICAR, as well as the AMPK inhibitor compound C. We found that phosphorylation of desnutrin at S406 was increased in cultured cells by AICAR treatment, but suppressed by compound C, paralleling phosphorylation of AMPK and ACC (Figure 4E). We next measured the TAG hydrolase activity of WT desnutrin, the nonphosphorylatable S406A mutant, as well as the phosphorylation mimicking aspartate mutant (S406D). We found that TAG hydrolase activity of S406A and S406D mutant was decreased compared to WT desnutrin (Figure 4F). Moreover, by GST pull-down assay we found that mutation of S406 of desnutrin to either alanine or aspartate blocked interaction with 14-3-3, correlating with decreased lipase activity in these mutants (Figure 4G). Furthermore, immunoprecipitation of HEK293 cells cotransfected with WT desnutrin, S406A mutant, S406D mutant, or GFP control and Myc-tagged 14-3-3 showed an interaction of 14-3-3 with WT desnutrin, but not with the S406A or S406D mutants (Figure 4H). In this regard, previous studies have shown that serine to aspartate substitution, thought to mimic phosphorylated serine, are inactive in some cases for 14-3-3 proteins (Kaeser et al., 2008).

To determine the role of AMPK specifically on desnutrin-catalyzed lipolysis, we transfected WT desnutrin or S406A mutant into oleate-loaded HEK293 cells, which express a very low level of endogenous HSL. The AICAR treatment increased lipolysis by 1.8-fold in cells transfected with WT desnutrin, but failed to do so in S406A mutant transfected cells, indicating that AMPK-activation increases lipolysis via phosphorylation of S406 of desnutrin (Figure 4I).

Phosphorylation of Desnutrin by AMPK Increases Desnutrin-Catalyzed Lipolysis in Cultured Adipocytes and in an In Vivo Context in Mice

The effect of AMPK in regulating lipolysis in adipose tissue has been controversial (Daval et al., 2005; Yin et al., 2003). Since adipocytes express high levels of endogenous HSL, it is difficult to dissociate the effect of desnutrin on lipolysis from that of HSL (Figure S4E). To overcome this obstacle, we utilized adenovirus for high-level overexpression of WT desnutrin, S406A mutant desnutrin, or GFP control in differentiated 3T3-L1ΔCAR adipocytes stably expressing the gene-encoding coxsackie and adenovirus receptor (Orlicky et al., 2001). We found that overnight pretreatment with AICAR increased lipolysis by 50% in control adipocytes. Desnutrin levels were unchanged during

(F) In vitro TAG hydrolase activity in BAT of mice upon cold exposure and western blotting for desnutrin (inset).
(G) Oxygen consumption rate (VO_2) measured through indirect calorimetry.
(H) VO_2 after intraperitoneal injection of CL316243.
(I) FA oxidation in white (left) and brown (right) adipocytes (n = 4). Data are expressed as means ± SEM. *p < 0.05, **p < 0.01, ***p < 0.001.

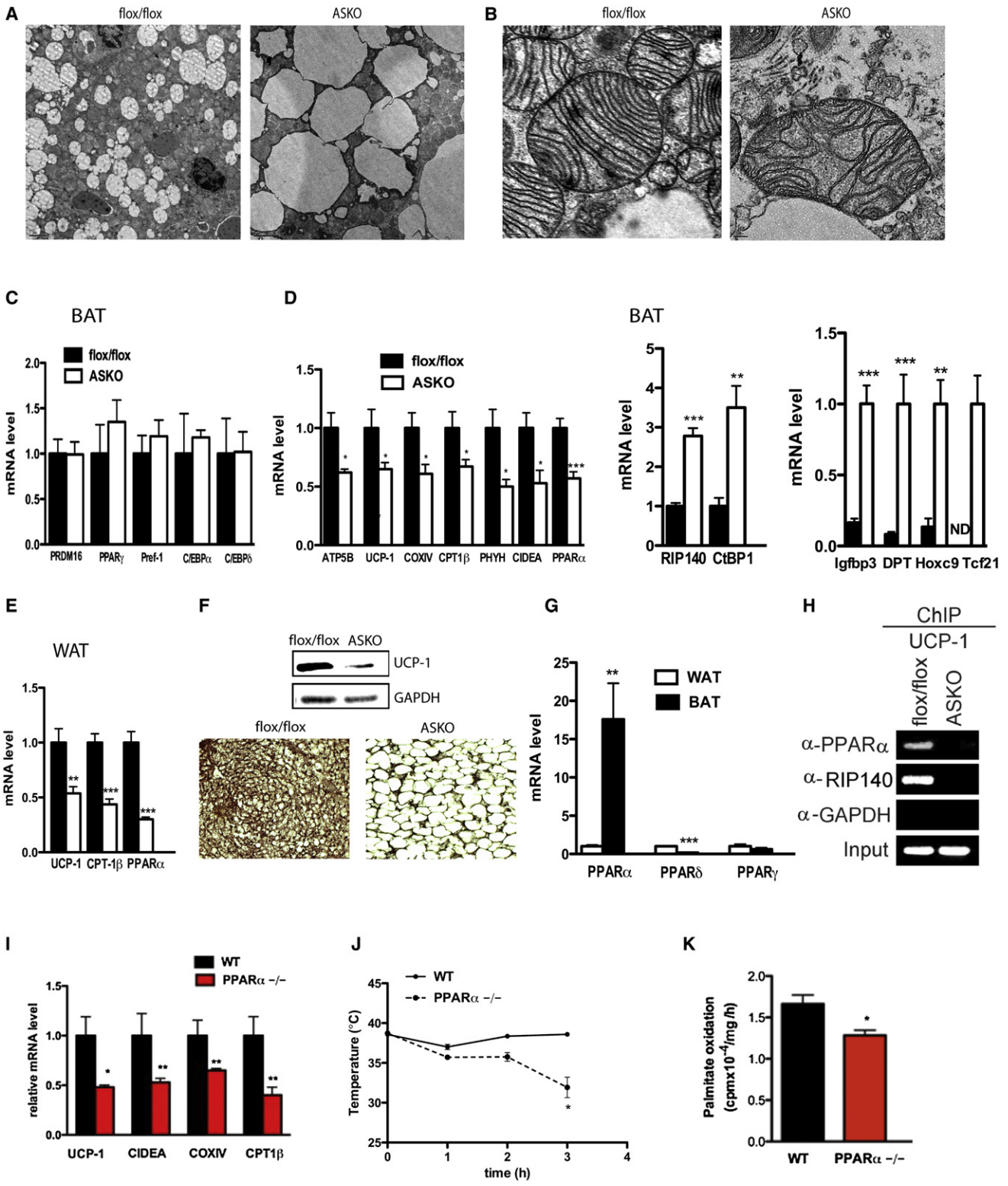

Figure 3. Desnutrin Ablation Converts of BAT to a WAT-like Phenotype

(A and B) Transmission electron microscopy of BAT showing the lipid droplet, scale bar = 2 μm (A), or focused on mitochondria, scale bar = 0.2 μm (B).

(C) RT-qPCR of BAT (n = 5–10).

(D) RT-qPCR of BAT (n = 5–10) (ND = not detected).

(E) RT-qPCR of WAT (n = 5–10).

the entire treatment period (Figures 4J and S4A). Furthermore, in response to AICAR treatment, we found that only WT desnutrin, and not the S406A mutant, showed an increase in lipolysis above control levels, clearly demonstrating that AMPK phosphorylation of desnutrin at S406 increases lipolysis in adipocytes (Figure 4J).

To test the effect of AMPK on lipolysis in vivo, we next administered AICAR intraperitoneally to flox/flox and desnutrin-ASKO mice. Five hours after injection, we detected that AICAR increased serum FA levels in control, flox/flox mice but not in desnutrin-ASKO mice, indicating that the AMPK-mediated increase in lipolysis is desnutrin dependent (Figure 4K). We also examined effects of chronic AICAR treatment. After 3 weeks of AICAR treatment, expression of genes involved in FA oxidation, PPARα and CPT1β, was induced in adipose tissue of flox/flox mice, but not in desnutrin-ASKO mice (Figure 4L).

To further address the biological significance of S406 phosphorylation of desnutrin, we performed tail vein injection of adenovirus of WT desnutrin, S406A mutant, and control GFP into mice. While TAG hydrolase activity was increased in the livers of WT desnutrin-infected mice compared to control virus-infected mice, the activity remained low in the livers of S406A mutant-injected mice (Figure 4M). Hepatic TAG levels were drastically decreased in WT desnutrin-infected mice as compared to control-GFP adenovirus-injected mice, as determined by TAG content and by sectioning and staining with oil red O (Figure 4N). In contrast, hepatic TAG levels were only marginally decreased in the livers of S406A mutant-infected mice (Figure 4N).

DISCUSSION

Impaired BAT function in our desnutrin-ASKO mice can be attributed to (1) decreased expression of oxidative and thermogenic genes and (2) severely blunted lipolysis that lowers FAs, preventing UCP-1 activation and decreasing FA oxidation. Notably, the conversion of BAT to a WAT-like tissue observed in desnutrin-ASKO mice does not appear to be due to decreased lipolysis in general, since opposing changes in BAT were observed in other mouse models with altered lipolysis. HSL null mice had an enhancement of BAT-like features in WAT, while mice overexpressing perilipin in adipose tissue with blunted lipolysis exhibited increased expression of oxidative genes in BAT (Miyoshi et al., 2010; Strom et al., 2008). Furthermore, unlike HSL null mice, desnutrin-ASKO mice exhibit a phenotype similar to β-adrenergic receptor-ablated mice (Bachman et al., 2002; Strom et al., 2008). These findings establish that desnutrin-catalyzed lipolysis is a major determinant of thermogenesis, required for a BAT phenotype, and that different lipases may regulate distinct metabolic pathways. In this regard, our previous studies on transgenic mice overexpressing desnutrin in adipose tissue also showed increased expression of UCP-1 and other oxidative genes in WAT with high FA oxidation within adipocytes.

Recently, it has been reported that WAT and BAT are intermingled in a single fat depot of rodents and may be capable of so called "transdifferentiation" or "browning," as observed by increased BAT-like properties during cold exposure (Barbatelli et al., 2010; Frontini and Cinti, 2010). While de novo differentiation of precursor cells could occur, this is unlikely, since we did not detect any differences in PRDM16 expression in BAT from desnutrin-ASKO mice, nor did we detect any changes in the morphology of BAT during embryonic development (Frontini and Cinti, 2010). While the mechanism underlying "transdifferentiation" is not known, desnutrin-catalyzed lipolysis may play an important role in the plasticity of adipocytes, conceivably by providing ligands for binding/activation of PPARα. Lower PPARα binding to the UCP-1 promoter in BAT of desnutrin-ASKO mice is consistent with other reports showing reduced PPARα binding to its target genes upon decreased ligand availability (Mandard et al., 2004; van der Meer et al., 2010). Although PPARγ can bind to the same enhancer region of the UCP-1 promoter (Barbera et al., 2001), it has been proposed that PPARγ may play a more important role during BAT development, while PPARα may be critical for function of mature BAT (Villarroya et al., 2007). Accordingly, we found that only PPARα is expressed at a much higher level in BAT compared to WAT. We also found that PPARα null mice have decreased expression of UCP-1 and other oxidative and thermogenic genes, with impaired thermogenesis. This is in contrast with reported PPARγ null mice having normal UCP-1 levels in BAT with functional thermogenesis (He et al., 2003).

Upon cold exposure or β-adrenergic stimulation, AMPK activity in BAT has been reported to increase, suggesting its role in regulating thermogenesis through activation of AMPK by PKA (Mulligan et al., 2007). However, this is controversial, with some reports showing activation of AMPK by PKA and others showing inhibition (Djouder et al., 2010; Omar et al., 2009). Furthermore, the role of AMPK in the regulation of lipolysis has also been controversial (Daval et al., 2005; Yin et al., 2003). Here, we found that AMPK phosphorylates S406 of desnutrin to increase its activity and promote lipolysis. Our results predict that, during cold exposure, AMPK may phosphorylate desnutrin, stimulating TAG hydrolase activity and thermogenesis. Our findings that cold exposure induces TAG hydrolase activity in BAT without changing desnutrin expression and that this cold-induced increase in TAG hydrolase activity was blunted in desnutrin-ASKO mice are consistent with the notion that desnutrin is regulated by posttranslational modification in BAT during cold exposure. Our findings are also in line with the well-established role of AMPK as a cellular energy sensor. If AMPK increases FA oxidation, it is logical that FA substrates must be increased. In support of this idea, our current studies as well as previous studies on transgenic mice overexpressing desnutrin in adipose tissue show that desnutrin-catalyzed lipolysis promotes FA oxidation. It is conceivable that AMPK may

(F) Western blotting (upper) and immunostaining (lower) for UCP-1 in BAT.
(G) RT-qPCR for PPARα, δ, and γ in WAT and BAT of WT mice (n = 3–5).
(H) Chromatin immunoprecipitation (ChIP) using a PPARα, RIP140, or control GAPDH antibody for binding to the UCP-1 promoter.
(I) RT-qPCR in BAT of PPARα null mice (n = 4–5).
(J) Body temperature of WT and PPARα null mice exposed to 4°C in the fasted state (n = 4).
(K) FA oxidation in white adipocytes from WT and PPARα null mice. Data are expressed as means ± SEM. *$p < 0.05$, **$p < 0.01$, ***$p < 0.001$.

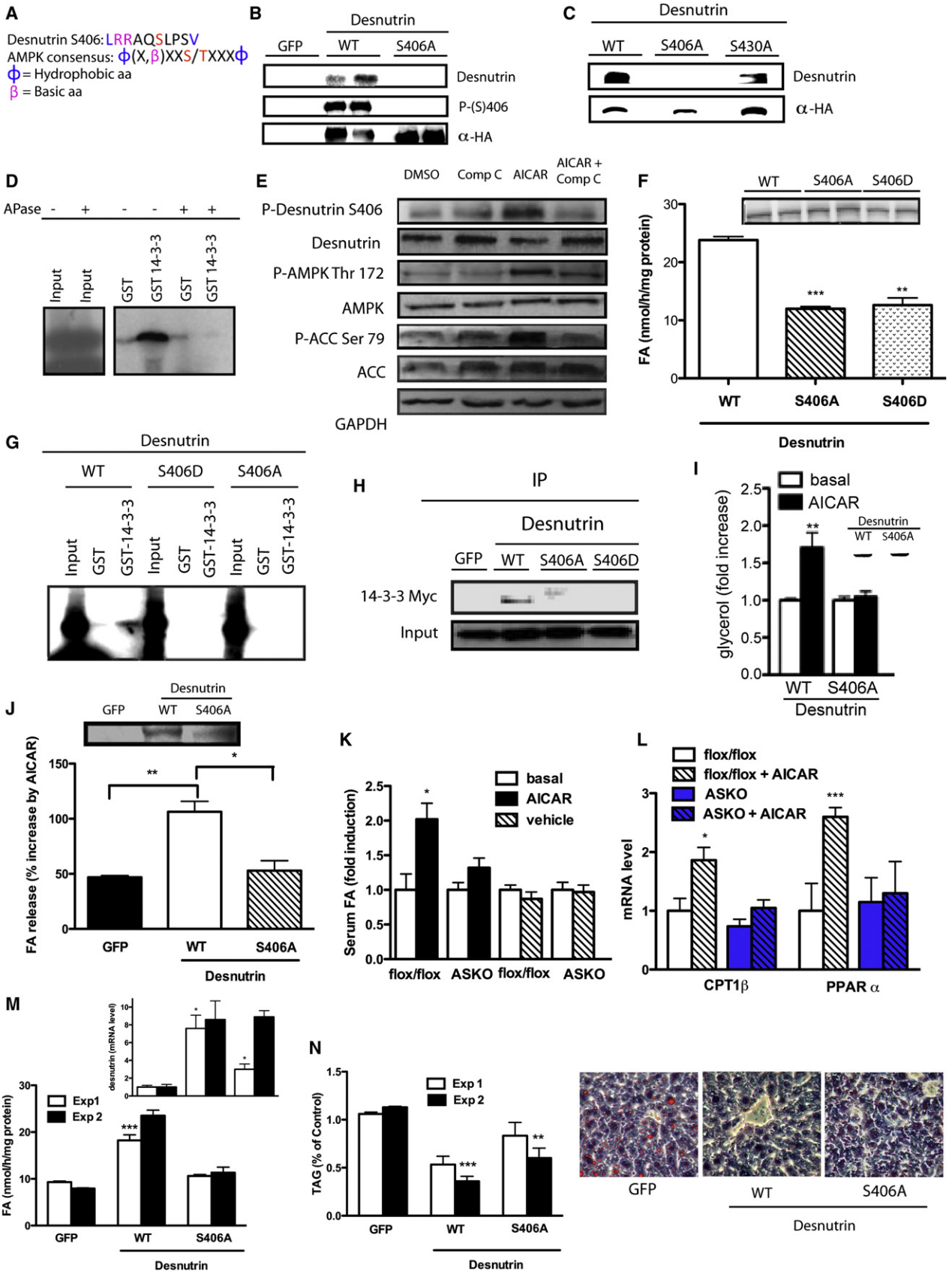
A
Desnutrin S406: LRRAQSLPSV
AMPK consensus: ϕ(X,β)XXS/TXXXϕ
ϕ = Hydrophobic aa
β = Basic aa
B
Desnutrin
GFP
WT
S406A
Desnutrin
P-(S)406
α-HA
C
Desnutrin
WT
S406A
S430A
Desnutrin
α-HA
D
APase - + - - + +
Input
Input
GST
GST 14-3-3
GST
GST 14-3-3
E
DMSO
Comp C
AICAR
AICAR + Comp C
P-Desnutrin S406
Desnutrin
P-AMPK Thr 172
AMPK
P-ACC Ser 79
ACC
GAPDH
F
WT
S406A
S406D
FA (nmol/h/mg protein)
WT
S406A
S406D
Desnutrin
G
Desnutrin
WT
S406D
S406A
Input
GST
GST-14-3-3
H
IP
Desnutrin
GFP
WT
S406A
S406D
14-3-3 Myc
Input
I
basal
AICAR
Desnutrin
WT
S406A
glycerol (fold increase)
WT
S406A
Desnutrin
J
Desnutrin
GFP
WT
S406A
FA release (% increase by AICAR)
GFP
WT
S406A
Desnutrin
K
basal
AICAR
vehicle
Serum FA (fold induction)
flox/flox
ASKO
flox/flox
ASKO
L
flox/flox
flox/flox + AICAR
ASKO
ASKO + AICAR
mRNA level
CPT1β
PPAR α
M
Exp1
Exp 2
desnutrin (mRNA level)
FA (nmol/h/mg protein)
GFP
WT
S406A
Desnutrin
N
Exp 1
Exp 2
TAG (% of Control)
GFP
WT
S406A
Desnutrin
GFP
WT
S406A
Desnutrin

increase FA oxidation, in part, via activation of desnutrin (Ahmadian et al., 2009b). Our observation that chronic AICAR administration induced expression of PPARα and CPT1β in control mice but not in desnutrin-ASKO mice further links AMPK-desnutrin-PPARα to increased FA oxidation and UCP-1 induction for thermogenesis. In this regard, we previously reported that mice lacking AMPKα2 are obese with adipocyte hypertrophy (Villena et al., 2004b). Since even a modest amount of BAT may account for a significant portion of daily energy expenditure (Frühbeck et al., 2009), strategies designed at targeting AMPK phosphorylation/activation of desnutrin might offer promising therapeutic approaches for obesity and related disorders.

EXPERIMENTAL PROCEDURES

Generation of Desnutrin-ASKO Mice and Mouse Maintenance

All studies received approval from the University of California at Berkeley Animal Care and Use Committee. Generation and maintenance of various mouse strains are described in detail in the Supplemental Experimental Procedures.

Antibody Generation, Immunoblotting, and Immunoprecipitation

Desnutrin antibody was raised in rabbits against the C-terminal amino acids of desnutrin (TAADPATPQDPPGLPPC). Use of various antibodies in immunoblotting and immunoprecipitation is described in detail in the Supplemental Experimental Procedures.

Chromatin Immunoprecipitation

BAT isolation, fixation, and ChIP are described in detail in the Supplemental Experimental Procedures.

RNA Extraction and Real-Time RT-PCR

Total RNA was prepared using TRIzol Reagent (Invitrogen), and cDNA was synthesized from 2.5 μg of RNA by Superscript II reverse transcriptase (Invitrogen). Gene expression was determined by RT-qPCR performed with an ABI PRISM7700 sequence fast detection system (Applied Biosystems) and was quantified by measuring the threshold cycle normalized to GAPDH, then expressed relative to flox/flox controls. Custom primers and probes are given in the Supplemental Information.

In Vitro Phosphorylation and TAG Hydrolase Activity Assays

In vitro phosphorylation and TAG hydrolase activity assays were performed as described in the Supplemental Experimental Procedures.

GST Pull-Down Assay

Production of GST-fusion proteins by overexpression in *E. coli*, generation of in vitro translation products, and GST pull-down assay are described in the Supplemental Experimental Procedures.

Adipocyte Isolation, Size Determination, Cryosectioning, and Transmission Electron Microscopy

Gonadal fat samples and intrascapular BAT were used for adipocyte isolation. Cell size measurement, cryosectioning, and transmission electron microscopy were performed as described in the Supplemental Experimental Procedures.

Adipose Lipolysis and FA Oxidation

Lipolysis using adipose explants and isolated adipocytes and FA oxidation in isolated adipocytes were determined as described in the Supplemental Experimental Procedures.

Glucose and Insulin Tolerance Tests and Hyperinsulinemic-Euglycemic Clamp

For the GTT, we intraperitoneally injected mice with D-glucose (2 mg/g body weight) after an overnight fast and monitored tail blood glucose levels. For ITT, mice were intraperitoneally injected with insulin (humulin, Eli Lilly) (0.75 mU/g body weight) after a 5 hr fast. Hyperinsulinemic-euglycemic clamp procedures are described in the Supplemental Experimental Procedures.

^2H_2O Labeling and GCMS Analysis of TAG-Glycerol and TAG-FA and Calculation of All-Source TAG Turnover and Palmitate Turnover

The detailed methods and calculation are described in the Supplemental Experimental Procedures.

Indirect Calorimetry and Body Temperature

Oxygen consumption (VO_2) was measured using the Comprehensive Laboratory Animal Monitoring System (CLAMS; Columbus, OH). Data were normalized to body weights. Body temperatures were assessed in 25-week-old male mice using a RET-3 rectal probe for mice (Physitemp). CL316243 (Sigma) was intraperitoneally injected into mice at 1 mg/kg body weight.

TAG and DAG Extraction and Metabolite Measurements

Extractions and metabolite measurements were performed as described in the Supplemental Experimental Procedures.

Statistical Analyses

Data are expressed as means ± SEM. Statistically significant differences between two groups were assessed by Student's t test.

Figure 4. Desnutrin Is Phosphorylated by AMPK to Increase Lipolysis

(A) AMPK consensus motif and murine desnutrin S406.
(B) Autoradiography to detect phosphorylated desnutrin after in vitro phosphorylation and western blot using a phospho-14-3-3 antibody to detect phosphorylation of S406 of desnutrin (middle) and HA antibody to detect total desnutrin protein (lower).
(C) Autoradiography for phosphorylated desnutrin and western blot using an HA antibody for total desnutrin.
(D) GST pull-down assay with in vitro translated desnutrin and GST-14-3-3 with or without alkaline phosphatase treatment (APase).
(E) Western blot for phospho-desnutrin at S406A, phospho-AMPK at Thr172, and phospho-ACC at Ser79 in WT desnutrin-transfected HEK293 cells treated with compound C and AICAR.
(F) TAG hydrolase assay and western blot showing desnutrin overexpression (inset).
(G) GST pull-down of in vitro-translated WT or desnutrin mutants with GST-14-3-3.
(H) Cotransfection followed by coimmunoprecipitation of 14-3-3-Myc with WT or desnutrin mutant.
(I) Glycerol release from HEK293 cells transfected with WT or S406A desnutrin, treated with or without AICAR.
(J) FA release from differentiated 3T3-L1ΔCAR adipocytes infected with WT desnutrin, S406A mutant, or GFP control adenovirus after pretreatment with AICAR, and western blot showing overexpression (inset).
(K) Serum FA levels after injection with AICAR.
(L) RT-qPCR for CPT1β and PPARα from gonadal WAT (n = 5).
(M and N) In vitro TAG hydrolase activities. TAG levels (left) and cryosectioning and staining with oil red O (right) of the livers of HFD-fed WT mice infected with WT desnutrin, S406A mutant, or GFP control adenovirus. Expression levels of WT desnutrin and S406A mutant upon adenovirus injection in liver by RT-qPCR are shown in inset. Data are expressed as means ± SEM. *$p < 0.05$, **$p < 0.01$, ***$p < 0.001$.

SUPPLEMENTAL INFORMATION

Supplemental Information includes Supplemental Experimental Procedures, Supplemental References, four figures, and one table and can be found with this article online at doi:10.1016/j.cmet.2011.05.002.

ACKNOWLEDGMENTS

This work was supported in part by DK75682 (H.S.S.), DK40936 (G.I.S.), and U24 DK076169 (V.T.S. and G.I.S.) from the National Institutes of Health. The authors thank R. Wong, A. Thompson, G. Wong, T. Liu, R. Mantara, T. Voortman, and E. Morse for technical and graphical assistance; A. Stahl and M. Kazantzis for help in metabolic chamber experiments; and A. Bradley for providing the pFlexible plasmid.

Received: August 2, 2010
Revised: December 15, 2010
Accepted: March 23, 2011
Published: June 7, 2011

REFERENCES

Ahmadian, M., Duncan, R.E., and Sul, H.S. (2009a). The skinny on fat: lipolysis and fatty acid utilization in adipocytes. Trends Endocrinol. Metab. *20*, 424–428.

Ahmadian, M., Duncan, R.E., Varady, K.A., Frasson, D., Hellerstein, M.K., Birkenfeld, A.L., Samuel, V.T., Shulman, G.I., Wang, Y., Kang, C., and Sul, H.S. (2009b). Adipose overexpression of desnutrin promotes fatty acid use and attenuates diet-induced obesity. Diabetes *58*, 855–866.

Bachman, E.S., Dhillon, H., Zhang, C.Y., Cinti, S., Bianco, A.C., Kobilka, B.K., and Lowell, B.B. (2002). betaAR signaling required for diet-induced thermogenesis and obesity resistance. Science *297*, 843–845.

Barbatelli, G., Murano, I., Madsen, L., Hao, Q., Jimenez, M., Kristiansen, K., Giacobino, J.P., De Matteis, R., and Cinti, S. (2010). The emergence of cold-induced brown adipocytes in mouse white fat depots is determined predominantly by white to brown adipocyte transdifferentiation. Am. J. Physiol. Endocrinol. Metab. *298*, E1244–1253.

Barbera, M.J., Schluter, A., Pedraza, N., Iglesias, R., Villarroya, F., and Giralt, M. (2001). Peroxisome proliferator-activated receptor alpha activates transcription of the brown fat uncoupling protein-1 gene. A link between regulation of the thermogenic and lipid oxidation pathways in the brown fat cell. J. Biol. Chem. *276*, 1486–1493.

Cannon, B., and Nedergaard, J. (2004). Brown adipose tissue: function and physiological significance. Physiol. Rev. *84*, 277–359.

Daval, M., Diot-Dupuy, F., Bazin, R., Hainault, I., Viollet, B., Vaulont, S., Hajduch, E., Ferré, P., and Foufelle, F. (2005). Anti-lipolytic action of AMP-activated protein kinase in rodent adipocytes. J. Biol. Chem. *280*, 25250–25257.

Djouder, N., Tuerk, R.D., Suter, M., Salvioni, P., Thali, R.F., Scholz, R., Vaahtomeri, K., Auchli, Y., Rechsteiner, H., Brunisholz, R.A., et al. (2010). PKA phosphorylates and inactivates AMPKalpha to promote efficient lipolysis. EMBO J. *29*, 469–481.

Duncan, R.E., Ahmadian, M., Jaworski, K., Sarkadi-Nagy, E., and Sul, H.S. (2007). Regulation of lipolysis in adipocytes. Annu. Rev. Nutr. *27*, 79–101.

Frontini, A., and Cinti, S. (2010). Distribution and development of brown adipocytes in the murine and human adipose organ. Cell Metab. *11*, 253–256.

Frühbeck, G., Becerril, S., Sáinz, N., Garrastachu, P., and García-Velloso, M.J. (2009). BAT: a new target for human obesity? Trends Pharmacol. Sci. *30*, 387–396.

Haemmerle, G., Lass, A., Zimmermann, R., Gorkiewicz, G., Meyer, C., Rozman, J., Heldmaier, G., Maier, R., Theussl, C., Eder, S., et al. (2006). Defective lipolysis and altered energy metabolism in mice lacking adipose triglyceride lipase. Science *312*, 734–737.

He, W., Barak, Y., Hevener, A., Olson, P., Liao, D., Le, J., Nelson, M., Ong, E., Olefsky, J.M., and Evans, R.M. (2003). Adipose-specific peroxisome proliferator-activated receptor gamma knockout causes insulin resistance in fat and liver but not in muscle. Proc. Natl. Acad. Sci. USA *100*, 15712–15717.

Jenkins, C.M., Mancuso, D.J., Yan, W., Sims, H.F., Gibson, B., and Gross, R.W. (2004). Identification, cloning, expression, and purification of three novel human calcium-independent phospholipase A2 family members possessing triacylglycerol lipase and acylglycerol transacylase activities. J. Biol. Chem. *279*, 48968–48975.

Kaeser, P.S., Kwon, H.B., Blundell, J., Chevaleyre, V., Morishita, W., Malenka, R.C., Powell, C.M., Castillo, P.E., and Südhof, T.C. (2008). RIM1alpha phosphorylation at serine-413 by protein kinase A is not required for presynaptic long-term plasticity or learning. Proc. Natl. Acad. Sci. USA *105*, 14680–14685.

Kim, S.C., Chen, Y., Mirza, S., Xu, Y., Lee, J., Liu, P., and Zhao, Y. (2006). A clean, more efficient method for in-solution digestion of protein mixtures without detergent or urea. J. Proteome Res. *5*, 3446–3452.

Lage, R., Diéguez, C., Vidal-Puig, A., and López, M. (2008). AMPK: a metabolic gauge regulating whole-body energy homeostasis. Trends Mol. Med. *14*, 539–549.

Mandard, S., Zandbergen, F., Tan, N.S., Escher, P., Patsouris, D., Koenig, W., Kleemann, R., Bakker, A., Veenman, F., Wahli, W., et al. (2004). The direct peroxisome proliferator-activated receptor target fasting-induced adipose factor (FIAF/PGAR/ANGPTL4) is present in blood plasma as a truncated protein that is increased by fenofibrate treatment. J. Biol. Chem. *279*, 34411–34420.

Miyoshi, H., Souza, S.C., Endo, M., Sawada, T., Perfield, J.W., 2nd, Shimizu, C., Stancheva, Z., Nagai, S., Strissel, K.J., Yoshioka, N., et al. (2010). Perilipin overexpression in mice protects against diet-induced obesity. J. Lipid Res. *51*, 975–982.

Mulligan, J.D., Gonzalez, A.A., Stewart, A.M., Carey, H.V., and Saupe, K.W. (2007). Upregulation of AMPK during cold exposure occurs via distinct mechanisms in brown and white adipose tissue of the mouse. J. Physiol. *580*, 677–684.

Narbonne, P., and Roy, R. (2009). Caenorhabditis elegans dauers need LKB1/AMPK to ration lipid reserves and ensure long-term survival. Nature *457*, 210–214.

Omar, B., Zmuda-Trzebiatowska, E., Manganiello, V., Göransson, O., and Degerman, E. (2009). Regulation of AMP-activated protein kinase by cAMP in adipocytes: roles for phosphodiesterases, protein kinase B, protein kinase A, Epac and lipolysis. Cell. Signal. *21*, 760–766.

Orlicky, D.J., DeGregori, J., and Schaack, J. (2001). Construction of stable coxsackievirus and adenovirus receptor-expressing 3T3-L1 cells. J. Lipid Res. *42*, 910–915.

Strom, K., Hansson, O., Lucas, S., Nevsten, P., Fernandez, C., Klint, C., Moverare-Skrtic, S., Sundler, F., Ohlsson, C., and Holm, C. (2008). Attainment of brown adipocyte features in white adipocytes of hormone-sensitive lipase null mice. PLoS One *3*, e1793.

van der Meer, D.L., Degenhardt, T., Väisänen, S., de Groot, P.J., Heinäniemi, M., de Vries, S.C., Müller, M., Carlberg, C., and Kersten, S. (2010). Profiling of promoter occupancy by PPARalpha in human hepatoma cells via ChIP-chip analysis. Nucleic Acids Res. *38*, 2839–2850.

Villarroya, F., Iglesias, R., and Giralt, M. (2007). PPARs in the Control of Uncoupling Proteins Gene Expression. PPAR Res. *2007*, 74364.

Villena, J.A., Roy, S., Sarkadi-Nagy, E., Kim, K.H., and Sul, H.S. (2004a). Desnutrin, an adipocyte gene encoding a novel patatin domain-containing protein, is induced by fasting and glucocorticoids: ectopic expression of desnutrin increases triglyceride hydrolysis. J. Biol. Chem. *279*, 47066–47075.

Villena, J.A., Viollet, B., Andreelli, F., Kahn, A., Vaulont, S., and Sul, H.S. (2004b). Induced adiposity and adipocyte hypertrophy in mice lacking the AMP-activated protein kinase-alpha2 subunit. Diabetes *53*, 2242–2249.

Yin, W., Mu, J., and Birnbaum, M.J. (2003). Role of AMP-activated protein kinase in cyclic AMP-dependent lipolysis In 3T3-L1 adipocytes. J. Biol. Chem. *278*, 43074–43080.

Zimmermann, R., Strauss, J.G., Haemmerle, G., Schoiswohl, G., Birner-Gruenberger, R., Riederer, M., Lass, A., Neuberger, G., Eisenhaber, F., Hermetter, A., and Zechner, R. (2004). Fat mobilization in adipose tissue is promoted by adipose triglyceride lipase. Science *306*, 1383–1386.